analytical chemistry

pubs.acs.org/ac
Article

Transient Cross-linking Mass Spectrometry: Taking Conformational Snapshots of Proteins

Yuxin Xie,[1] Jiawen Wang,[1] Lei Yang,[1] Junjun Tao, Yuanyuan Xu, Yang Hu, Guiqing Zou, Yu Su, Meijun Liu, Huiyong Sun,* Haiping Hao,* Xiaowei Xu,* and Qiuling Zheng*

Cite This: *Anal. Chem.* 2025, 97, 5488−5497
Read Online
ACCESS | Metrics & More | Article Recommendations | Supporting Information

ABSTRACT: The dynamic nature of protein conformations is central to their biological functions. Conventional structural biology techniques provide static snapshots, whereas a comprehensive understanding requires an analysis of the dynamic conformations. In this study, we develop a transient cross-linking mass spectrometry method using a photo-cross-linker DCD. This cross-linker can be transiently activated to accomplish cross-linking, and with sample freezing, transient conformations are preserved, allowing temporal control and on-demand cross-linking. Its cross-linking site covers all amino acids, exhibiting diversity and providing rich structural information. Additionally, we develop a data-processing strategy by integrating a DCD-specific reporter ion and a defined ambiguous site annotation criterion, thereby ensuring the confidence in identification and cross-link site annotation. Thus, the developed transient cross-linking mass spectrometry, leveraging the distinctive features of DCD, has enabled us to analyze protein conformations and protein complexes with high resolution, take conformational snapshots, discern the coexistence of conformational intermediates, and decipher conformational fluctuations, shedding light on how proteins conformationally respond to biological signals and engage with interacting partners. Our results highlight DCD's potential for probing protein conformational changes, facilitating the elucidation of their pivotal roles within biological systems.

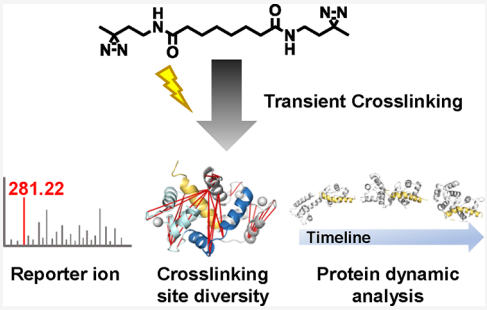

INTRODUCTION

The structure and dynamic properties of proteins are vital for their biological roles. Elucidating conformational changes and identifying new intermediate conformers are particularly valuable, providing insights into protein motion and interactions, shedding light on disease mechanisms, and informing drug design. Methods including X-ray crystallography and cryo-electron microscopy[1,2] are highly advantageous for high-resolution structural analysis but only provide static structures, missing the dynamic nature of proteins. Nuclear magnetic resonance spectroscopy (NMR) is applied for studying protein dynamics but is limited by its requirements for the sample amount and molecular size. Techniques such as fluorescence resonance energy transfer[3] or electron paramagnetic resonance[4] allow for dynamic analysis but require specific labeling and have spatial constraints. Mass spectrometry (MS)-based techniques are attracting increasing attention because of their high sensitivity and specificity. Native MS or affinity purification-based MS allows direct detection of proteins or protein complexes in their native states.[5,6] Coupling with hydrogen−deuterium exchange, hydroxyl radical footprinting or diethylpyrocarbonate surface labeling enables residue-level structural mapping,[7−10] yet these techniques face challenges to provide a comprehensive three-dimensional (3D) structural overview of proteins.

Chemical cross-linking MS is widely used for protein structural characterization and protein-protein interaction (PPI) analysis under a physiological environment.[11−14] Currently, cross-linkers targeting various amino acids have been developed, such as lysine, acidic amino acids, or cysteine;[15,16] however, the majority are *N*-hydroxysuccinimide (NHS) ester based and lysine specific. Yet, the resolution of structural analysis is constrained by the number and distribution of targetable sites within the cross-linking range. Photoreactive cross-linkers offer an advantage alternative, capable of achieving diversity of cross-linking,[17−20] for example, heterobifunctional cross-linkers that incorporate an NHS ester with a photoreactive moiety (e.g., diazirine or aryl azide). Beyond expanding the site diversity to obtain more structural information, analyzing the structural dynamics of proteins is also crucial, which requires that the cross-linking reaction be completed in a short period of time, ensuring that the protein's conformational changes are captured in a timely

Received: September 12, 2024
Revised: February 20, 2025
Accepted: February 24, 2025
Published: March 4, 2025

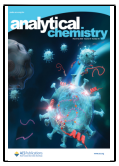

https://doi.org/10.1021/acs.analchem.4c04939
Anal. Chem. 2025, 97, 5488−5497

manner. However, the NHS ester-based cross-linking reaction typically requires 30 min or longer, which is not conducive to tracking protein conformational changes. For the aforementioned heterobifunctional cross-linkers, it requires a two-step procedure including NHS ester cross-linking followed up with UV irradiation (typically 15 to 50 min). There remains development of new cross-linkers with rapid reaction kinetics to trace protein conformational transitions, but the cross-linking site is limited to lysine residue.[12,21] Thus, it continues to be a significant challenge to achieve both purposes by one cross-linker.

In this study, we designed a new cross-linker named DCD, featuring two diazirine groups connected by a carbon chain. DCD can be transiently activated to achieve cross-linking, providing temporal control and enabling on-demand cross-linking. With a sample freezing, transient conformers or PPIs can be preserved for in situ cross-linking, while also improving the cross-linking efficiency. MS/MS analysis of the cross-link products yielded a DCD-specific reporter ion, which significantly improved the identification confidence and accuracy. The investigation into cross-linking sites revealed that DCD demonstrated cross-linking site diversity, delivering rich structural information and enabling a high-resolution structural analysis. These prompted us to develop a data-processing strategy, selecting the optimal data analysis software and fine-tuning parameters by incorporating the reporter ion, ambiguous site annotation, and solvent-accessible surface distance (SASD) measurements, thus simplifying the data interpretation process and greatly enhancing the accuracy of our analysis. Leveraging the unique advantages of DCD, we developed a transient cross-linking MS method, and it experimentally demonstrated the dynamic characteristics of the target protein and revealed the coexistence of conformational intermediates with high resolution. Consequently, DCD holds significant promise for the monitoring of conformational dynamics and characterization of PPIs.

METHODS AND MATERIALS

Reagents and Chemicals. Catalase and bovine serum albumin (BSA) were all purchased from Sigma-Aldrich (St Louis, Missouri, USA). Lysozyme was purchased from Sigma-Aldrich (St Louis, Missouri, USA) or MedChemExpress (Monmouth Junction, New Jersey, USA). A protein standard mixture, cross-linkers dithiobis(succinimidylpropionate) (DSP), disuccinimidyl glutarate (DSG), bis[sulfosuccinimidyl] suberate (BS^3), and sulfo-NHS-SS-diazirine (sulfo-SDAD) were all purchased from Thermo Fisher Scientific (Waltham, Massachusetts, USA). Calmodulin (CaM), peptide from CaMKII (sequence: LKKFNARRKLKGAILTTMLATRNFS), and model peptides were all purchased from Nanjing Peptide Industry (Nanjing, China). Melittin was purchased from Yien Chemical Technology (Shanghai, China). Cytochrome C was purchased from J&K Scientific (Beijing, China). Ubiquitin (Ub) was purchased from UB-biotech (Changchun, China). *Escherichia coli* 70S ribosome was purchased from New England Biolabs (Beverly, Massachusetts, USA).

DCD Cross-linking and Sample Processing. DCD was synthesized by our laboratory and verified by NMR and MS (Figures S1 and S2, respectively, and additional methods in the Supporting Information (SI). Peptides (2 mM) and DCD were mixed at a molar ratio of 1:10 (peptide:cross-linker). Model proteins were mixed with DCD at a molar ratio of 1:20 or a mass ratio of 1:1 (protein:cross-linker). For cross-linking of *E. coli* 70S ribosome and cell lysate, DCD was added at a final concentration of 2 mM. For cross-linking of CaM−target peptide complexes, Ca^{2+} was mixed with CaM at a molar ratio of 5:1. The target peptides were added at a ratio of 2:1 (target peptide:CaM), and DCD was added at a molar ratio of 1:20 (protein:cross-linker). Samples were stored in the Eppendorf tube, frozen by liquid nitrogen, placed at a distance of 10 cm from the laser, and irradiated for 60 s (wavelength: 355 nm, 120 μJ, Beijing Laserwave Optoelectronics Technology Co., Ltd.). The obtained cross-linked proteins underwent denaturation, DTT reduction, IAA alkylation, and enzymatic digestion prior to liquid chromatography (LC)-MS analysis (additional methods in the SI).

Data Processing. All cross-link results were obtained from three biological replicates. The identification of DCD cross-link products was performed by xiSEARCH (version 1.7.6.7)/pLink2 (version 2.3.10)/MeroX (version 2.0), as indicated. DSP, sulfo-SDAD, BS^3, and DSG cross-link product identification was performed by pLink2 (version 2.3.10). Regular proteomic analysis of cell lysate cross-linking was performed by PEAKS Studio (version 10.0). The major parameter settings are found in the Supporting Information. Protein structural modeling was conducted by molecular dynamics (MD) simulations (additional methods in the SI).

RESULTS AND DISCUSSION

Development of Transient Cross-linking Mass Spectrometry. Theoretically, DCD can be activated by laser irradiation without additional quenching due to its immediate reaction kinetics (within femtoseconds);[22] thus, one could expect a transient cross-linking with a broad amino acid reactivity. We first investigated DCD alone reacted under laser irradiation, which resulted in three primary products corresponding to the 4N elimination, followed by the insertion of two carbenes into a bond of the DCD chain (m/z 281.22), into a water molecule (m/z 299.23), and into two water molecules (m/z 317.24) (Figure S3A, possible reaction route shown in Figure S4A,B). Activating DCD in a frozen state with liquid nitrogen significantly reduced (m/z 299.23) or completely eliminated (m/z 317.24) side products, showing its high effectiveness in minimizing side reactions (Figure S3B). Additionally, we activated DCD and mixed it with a peptide mixture (SSTNVG and GCKNFFWK, denoted as SG and GK, respectively). No detection of peptide+DCD products demonstrated that the products from DCD reaction alone would not noncovalently bind to peptides, thereby avoiding interference with the identification of cross-link products (Figure S3C). Therefore, although we could not completely avoid the side reactions due to the high reactivity of carbene, these small molecules would not interfere with the cross-link identification and adversely affect structural analysis and could be effectively removed by ultrafiltration before enzymatic digestion at protein-level cross-linking.

Next, DCD cross-linking was performed on an SG and GK peptide mixture. Expected cross-link products were detected, including the singly charged ion of cross-linked SG (m/z 844.50), singly and doubly charged ions of cross-linked GK (m/z 1309.71 and 655.37, respectively), and singly and doubly charged ions of interpeptide cross-link product of SG and GK (m/z 1873.72 and 937.65, respectively) (Figure S5A), as well as cross-link products from DCD reaction alone, which would not be considered further. Focusing on the interpeptide cross-link product at m/z 937.65, the MS/MS spectrum yielded

https://doi.org/10.1021/acs.analchem.4c04939
Anal. Chem. 2025, 97, 5488−5497

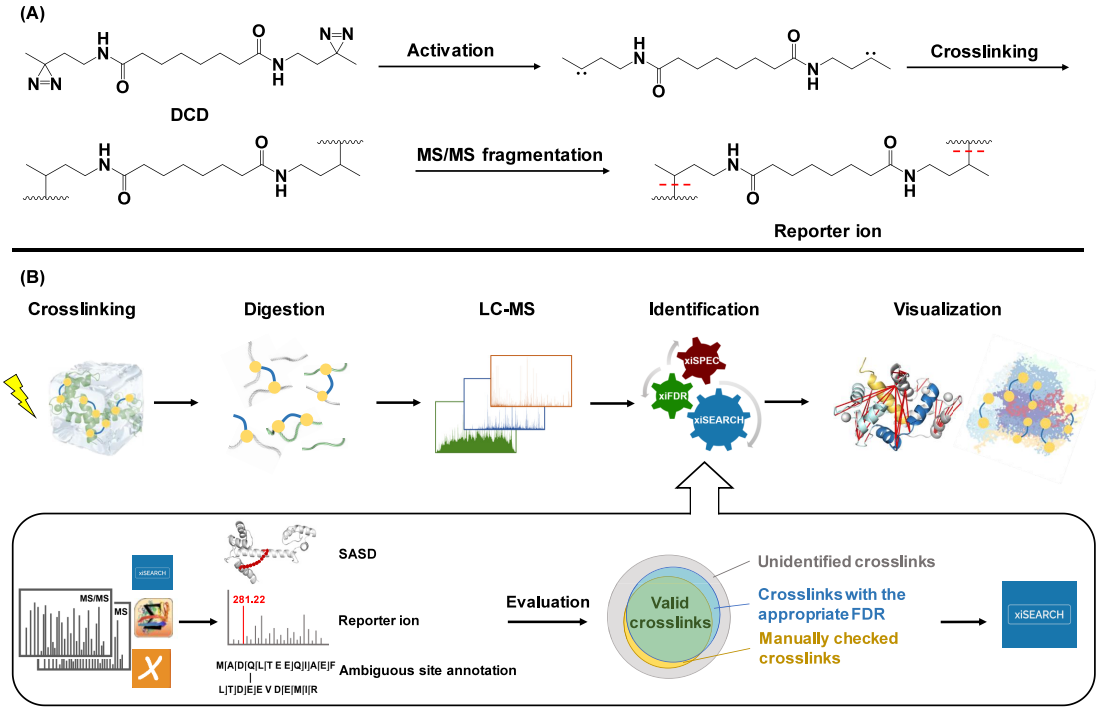

Figure 1. (A) Chemical structure of DCD, cross-linking reaction, and the generation of the reporter ion. (B) Workflow of the designed transient cross-linking MS, including DCD cross-linking, enzymatic digestion, LC-MS analysis, identification of cross-link products, and visualization.

fragment pairs of SG and GK+DCD, as well as GK and SG +DCD, along with a fragment ion at m/z 281.22, suggesting the cleavage of DCD in MS/MS analysis (Figure S5B). It could be attributed to a favored fragmentation process in which the DCD added by carbene modification was preferentially eliminated first (Figure 1A). A similar fragmentation pathway was also seen in other heterobifunctional NHS-diazirine cross-linkers.[20] We investigated DCD cross-linking of three more peptide mixtures, and the same fragment ions at m/z 281.22 were yielded in the MS/MS analysis of corresponding interpeptide cross-link products (Figure S6). Thus, we inferred that this diagnostic fragment ion m/z 281.22 can serve as a qualitative marker for cross-link product identification.

According to the DCD cross-linking chemistry, it resulted in an identical mass difference for dead-end and loop-link products (Figure S4C), which poses a challenge in their differentiation. Taking BSA as an example, after DCD cross-linking and enzymatic digestion, the obtained peptide mixture underwent LC-MS analysis and cross-link product identification. Focusing on peptide EATLEECCAKDDPHACY, it formed dead-end and loop-link products, which were separated by LC, eluting at 27.06 and 25.67 min, respectively. The MS/MS spectrum of the dead-end product yielded fragment ions y_{11} and y_{12}, confirming the dead-end modification at E_{382}. MS/MS analysis of the loop-link product yielded continuous y fragment ions, with no cleavage between H_{390} and A_{391}, indicating the formation of a loop link that hindered the MS/MS cleavage (Figure S7). Similar results were obtained for peptides SALTPDETYVPK and TCVADESHAGCEK, showing that their dead-end and loop-link products were separated. MS/MS spectra showed sufficient fragment ions for confirming their cross-link types, as well as for peptide sequencing and cross-link site annotation. More importantly, the same reporter ion was observed at m/z 281.22 for both cross-link products (Figures S8 and S9), confirming its presence in MS/MS spectra of all types of cross-link products and its reliability for subsequent data analysis.

The feasibility of DCD cross-linking was then investigated by reacting with model protein lysozyme. Upon transient activation (~1 s laser irradiation, Figure S10A), an additional protein distribution increased and was corroborated by deconvolution as DCD-cross-linked lysozyme. However, the cross-linking efficiency was relatively low due to the transient activation time, and the mass of cross-linked lysozyme (Δm = 308.3) also indicated a partial activation of DCD by losing only 2N (Figure S10B). We froze the sample with liquid nitrogen and investigated the laser irradiation time, ensuring to minimize unexpected protein structural alternations due to excessive laser energy while maintaining sample freezing and maximizing cross-linking efficiency. A total of 60 s of laser activation time led to a complete activation of DCD based on masses from deconvolution (Δm = 281.5, Figure S10C,D; lysozyme was cross-linked as monomer, verified by SDS-PAGE, Figure S10E). Besides diminishing side products, diazirine being activated in a frozen state enabled to extend the activation time while maintaining transient conformers, which showed an exclusive advantage in conducting in situ cross-linking and was applied for subsequent analysis (Figure 1B).

We then investigated the cross-linking site coverage and selectivity by conducting DCD cross-linking on cell lysates. The resulting data files were subjected to regular proteomic analysis by setting DCD as a variable modification. In this way, large-scale cross-linking site identification at the proteome level became feasible, and with such setting, dead-end products (+280.22 Da) were focused. Representative MS/MS spectra confirmed that these were dead-end products, with all amino acids cross-linkable by DCD and generating the same reporter ion at m/z 281.22 (Figures S11 and S12). A total of 753 modification sites from 114 identified proteins (molecular

https://doi.org/10.1021/acs.analchem.4c04939
Anal. Chem. 2025, 97, 5488−5497

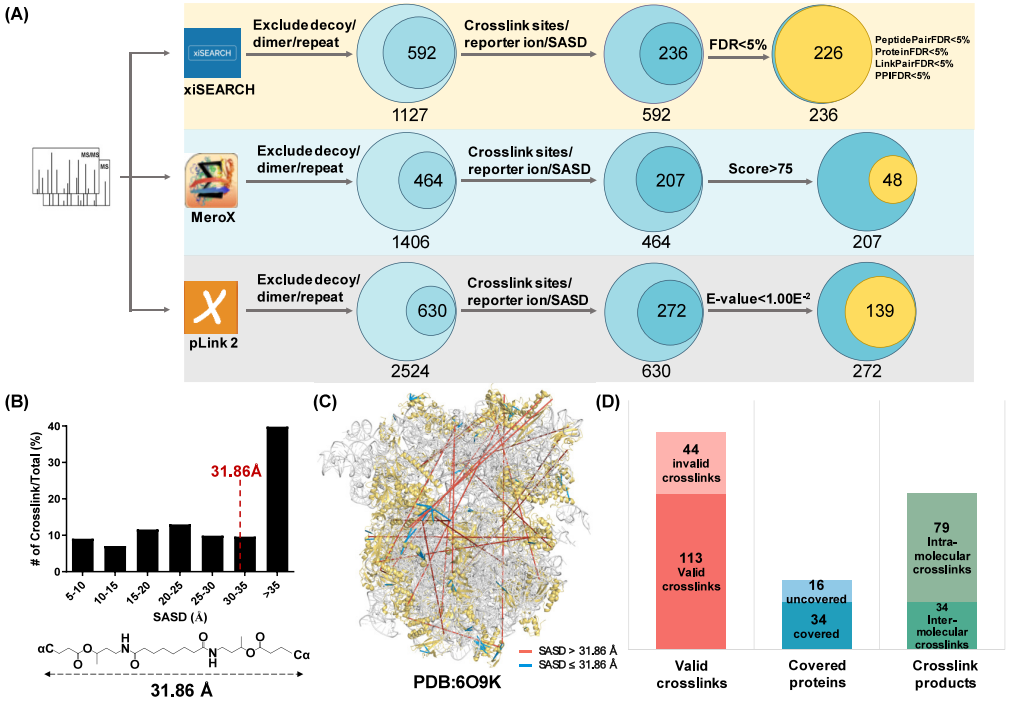

Figure 2. (A) Cross-link identification and software evaluation. (B) SASD measurement of cross-links from the training group. (C) DCD cross-linking of the *E. coli* 70S ribosome; blue lines indicated cross-links having SASD ≤ 31.86 Å, and orange red lines indicated cross-links having SASD > 31.86 Å. (D) Number of valid cross-links (indicating those having the reporter ion and satisfying the ambiguous site annotation criterion (n−n, $n \leq 3$), 113 cross-links), number of cross-linked proteins (34 proteins), and type of cross-link products (79 intramolecular and 34 intermolecular cross-links).

weight ranging from 7.8 to 534.2 kDa, sequence coverage ≥50%) were selected for statistical analysis, and the reporter ion for every cross-link product was manually checked. Results demonstrated that glutamic acid (E, 46.61%) had the highest cross-linking probability followed by aspartic acid (D, 10.23%), valine (V, 5.84%), tyrosine (Y, 4.78%), and glycine (G, 3.72%), aligning with previous studies that the generated diazo group had reactivity bias to carboxylic acids (D and E)[23] (Figure S13). Therefore, E was selected as the representative amino acid as it has a longer side chain, and the cross-linking constraint of DCD was measured as 31.86 Å (between two E residues, C_α−C_α distance). Notably, dead-end products reflect changes in surface accessibility, while loop-link products provide limited spatial information by connecting sequence-adjacent amino acids. In contrast, interpeptide cross-links provide the most valuable structural information and are the primary focus in typical cross-linking analysis. Consequently, subsequent database searching and identification process excluded loop-link and dead-end products, focusing on the identification of interpeptide cross-links, and they were presented in structural analysis. These results provide a fundamental basis for the further development and application of transient cross-linking.

Development of the Data Processing Strategy. DCD achieves the diversity of cross-linking while posing challenges for pinpointing the cross-link sites and for controlling the false discovery rate (FDR). For DCD cross-linking, having the benefit of the reporter ion generation, we proposed a data-processing strategy by integrating evaluation of MS/MS spectra, cross-linking constraint, and site annotation to improve the identification confidence and accuracy. We evaluated three widely used cross-link data analysis software, including MeroX, pLink2, and xiSEARCH, each of which has their independent criterion for cross-link identification, including Score >75 for MeroX,[24] *E*-value <1.00E^{-2} for pLink2,[25] and FDR < 5% for xiSEARCH.[26]

Nine sets of training data, namely, DCD-cross-linked BSA, Ca^{2+}−CaM, immunoglobulin G-binding protein A (gene: spa), immunoglobulin G-binding protein G (gene: spg), cytochrome C, catalase, Ca^{2+}−CaM−CaMKII binding peptide, Ca^{2+}-CaM-CaN binging peptide, and Ca^{2+}−CaM−melittin, were subjected to three selected software following their own criterion for cross-link identification. After excluding cross-links from decoy, dimer, and repeat, a total of 536 cross-links were identified by xiSEARCH, 295 by pLink2 and 85 by MeroX. Among the 536 cross-links identified by xiSEARCH, 516 contained the reporter ion, indicating a 96.27% accuracy rate of cross-link identification, which was 1.78 and 6.07 times higher compared to pLink2 and MeroX, respectively. Thus, xiSEARCH potentially emerged as a suitable search engine for DCD cross-linking. The annotation of DCD cross-linking sites was challenging due to its nonspecific reactivity, and insufficient fragmentation of large cross-links or those with low abundance. Taking cross-link product DAFL$_{350}$GSF-LKPDPNTLCDE$_{149}$F from BSA as an example, the sequence of peptide DAFLGSF was fully covered and the cross-link site was annotated at L_{350} by detecting fragment ions b_3 and y_3 (Figure S14A, in red). The other cross-link site was pinpointed at E_{149} by yielding fragment ions b_{10} and $[y_2+P]^{2+}$ (Figure S14A, in blue). In this case, fragment ions were sufficient for sequencing and pinpointing cross-link sites, thus yielding a highly credible identification result. For cross-link product LKPDPNTLCDE$_{149}$F-QTALVEL$_{555}$L, fragment ions were adequate for peptide sequencing, but the cross-linking sites were narrowed to E_{149}/F_{150} and L_{555}/L_{556} by observing b_{10} (in red) and b_6 (in blue) (Figure S14B). We defined this situation

https://doi.org/10.1021/acs.analchem.4c04939
Anal. Chem. 2025, 97, 5488−5497

as ambiguous site annotation, and the non-fragment window was denoted as $n-n$ (2−2 in this case), where n represents the number of consecutive amino acids that could be potential cross-link sites. We assessed more MS/MS spectra of cross-link products and realized that there were some cross-links that lack sufficient fragment ions for both peptide sequencing and cross-link site identification, for example cross-links DAFLGSFL$_{354}$Y-MPCTEDYL$_{476}$SL and SHCIAEVEKDAIPENLPPL-TAD$_{331}$FAEDKDVCK-APELLYYAN$_{182}$K (Figure S14C,D). Thus, to minimize the impact of imprecise annotation on structural analysis, we established a criterion that annotations within three consecutive amino acids be valid (denoted as $n-n$, $n \leq 3$), including the algorithm-annotated site, which had a smaller non-fragment window compared with others,[27] although it may exclude some potential cross-link products (e.g., having the reporter ion but with a larger non-fragment window).

To evaluate the reliability and precision of the identification, we conducted a critical screening that incorporated DCD-specific criteria, including the generation of the reporter ion, ambiguous site annotation ($n-n$, $n \leq 3$), and the alignment of DCD cross-linking constraint with SASD of cross-links (assessments based on PDB or AlphaFold structures). Accordingly, 226 cross-links from xiSEARCH passed the critical screening, which was 1.63 and 4.71 times higher than that of pLink2 (139 cross-links) and MeroX (48 cross-links), respectively. This confirmed the reliability of xiSEARCH for DCD cross-linking, as it identified the most valid cross-links with high confidence. We also reversed the identification process by performing critical screening followed up with software criteria evaluation in case some of the cross-link products were mistakenly excluded by software. A total of 272 cross-links were identified by pLink2, of which 139 had an E-value of <1.00E^{-2} (accounting for 51.10%). MeroX identified 207 cross-links, among which 48 had a score of >75 (accounting for 23.19%). As expected, xiSEARCH identified 236 cross-links, with 226 of these having FDR <5% (accounting for 95.76%), which placed xiSEARCH at the forefront among the three selected software. Thus, xiSEARCH was chosen for further data analysis (Figure 2A).

Comparing SASDs with known protein structures revealed that some cross-links surpassed DCD cross-linking constraints, termed overlength cross-links (Figure 2B). In practical cases, SASD measurement is not always feasible, especially for PPIs or proteins without PDB or AlphaFold structures. In addition, overlength cross-links are valuable for modeling and structural analysis, as they reflect protein dynamics.[13] Thus, we removed the SASD comparison from our assessment criteria and re-evaluated the reliability of xiSEARCH identification. Unlike other identification software, xiSEARCH offers the unique feature to set a four-level FDR, encompassing levels for peptide spectral matches (PSM), peptide pair, residue pairs, and protein pairs. Taking BSA as an example, critical screening resulted in 35 cross-links. By setting four-level FDR <5% in xiSEARCH, 65 cross-links were identified. Among these, 52 contained the reporter ion and satisfied the requirement for ambiguous site annotation, and 33 were identical to those identified by critical screening, indicating that setting four-level FDR <5% in xiSEARCH was highly accurate in cross-link identification (Table S1). Similarly, for cross-linking of Ca^{2+}-CaM, xiSEARCH gave 49 candidates, among which 28 had the reporter ion and met the standard of the ambiguous site annotation. Nineteen out of 20 cross-links that resulted from critical screening were included (Table S1). For immunoglobulin G-binding protein A and immunoglobulin G-binding protein G, 88 and 60 cross-links were identified with high confidence by having the reporter ion and satisfied the ambiguous site annotation and covered 76.19 and 67.57% results from the critical screening, respectively (Table S1). For cytochrome C and catalase, critical screening resulted to fewer cross-links by kicking out those having overlength SASDs, which resulted to the relative lower overlap percentages between critical screening and xiSEARCH with a set of four-level FDR <5% (covered three out of five and two out of three identical cross-links, respectively, Table S1). In the case of protein complex cross-linking, including CaM-CaMKII binding peptide, CaM-melittin, and CaM-CaN binding peptide, most intra- and intermolecular cross-links from the critical screening were covered, confirming that xiSEARCH with a set of four-level FDR <5% was also suitable for protein complex cross-link identification (Table S1). Therefore, we selected xiSEARCH with a set of four-level FDR <5% for subsequent cross-link identification.

We further used DCD-cross-linked *E. coli* 70S ribosome to validate the identification strategy. xiSEARCH identified 157 cross-links, and we first manually checked their MS/MS spectra, validating the reporter ion and the ambiguous site annotation. For instance, in the MS/MS spectrum of the cross-link product AQLQE$_{107}$IAQTK-AADMTGADIE$_{122}$AMTR, fragment ions were sufficient for peptide sequencing, and cross-link sites were confidently pinpointed to E$_{107}$ (detecting b_4, y_5, and $[y_6+P]^{2+}$, in red, Figure S15A) and E$_{122}$ (detecting y_4 and $[y_5+P]^{2+}$, in blue, Figure S15A), leading to an ambiguous site annotation of 1−1. For cross-link product SAGTY$_{160}$VQIVAR-AT$_{190}$LGEVGNAEHMLR, the reporter ion was observed and fragment ions were sufficient for sequencing. One of the cross-link sites was pinpointed to Y$_{160}$ by detecting b_4 and $[b_5+P]^{3+}$ (peptide SAGTY$_{160}$VQIVAR, in red, Figure S15B), while the other one could be A$_{189}$ or T$_{190}$ by detecting fragment ions of y_{12} and $[b_2+P]^{5+}$ (peptide AT$_{190}$LGEVGNAEHMLR, in blue, Figure S15B). Similar ambiguous site annotation could be observed for cross-link VM$_{48}$NMQAK-EAPLAIELDHD$_{45}$K. For VM$_{48}$NMQAK, the cross-link site could be V$_{47}$ or M$_{48}$ by detecting the fragment ion of y_5 (in red, Figure S15C). For EAPLAIELDHD$_{45}$K, the cross-link site was limited to H$_{44}$, D$_{45}$, and K$_{46}$ by detecting the fragment ion of b_9 without further confirmation (in blue, Figure S15C), leading to an ambiguous site annotation of 2−3. In addition, we also carefully examined MS/MS spectra of cross-links that had ambiguous site annotation larger than 4 ($n \geq 4$) at either side and found that most of them had insufficient fragmentation for sequencing or cross-link site annotation and were excluded from the identification list. These results confirmed that our set of ambiguous site annotation criterion ensured the confidence and accuracy of cross-link site identification and cross-link product sequencing.

On this basis, out of 157 cross-links, 113 were identified as valid (accounted for 71.97%) by having the reporter ion and satisfying the ambiguous site annotation criterion ($n-n$, $n \leq 3$), approving a high identification confidence provided by xiSEARCH. It included 79 intramolecular and 34 intermolecular cross-links, covering 34 proteins (total 50 proteins, PDB: 6O9K). Among the 113 cross-links, 87 of them were within the distance criterion (accounted for 76.99%), suggesting a high structural compatibility obtained from DCD cross-linking (Figure 2C,D and Table S2). These results

https://doi.org/10.1021/acs.analchem.4c04939
Anal. Chem. 2025, 97, 5488−5497

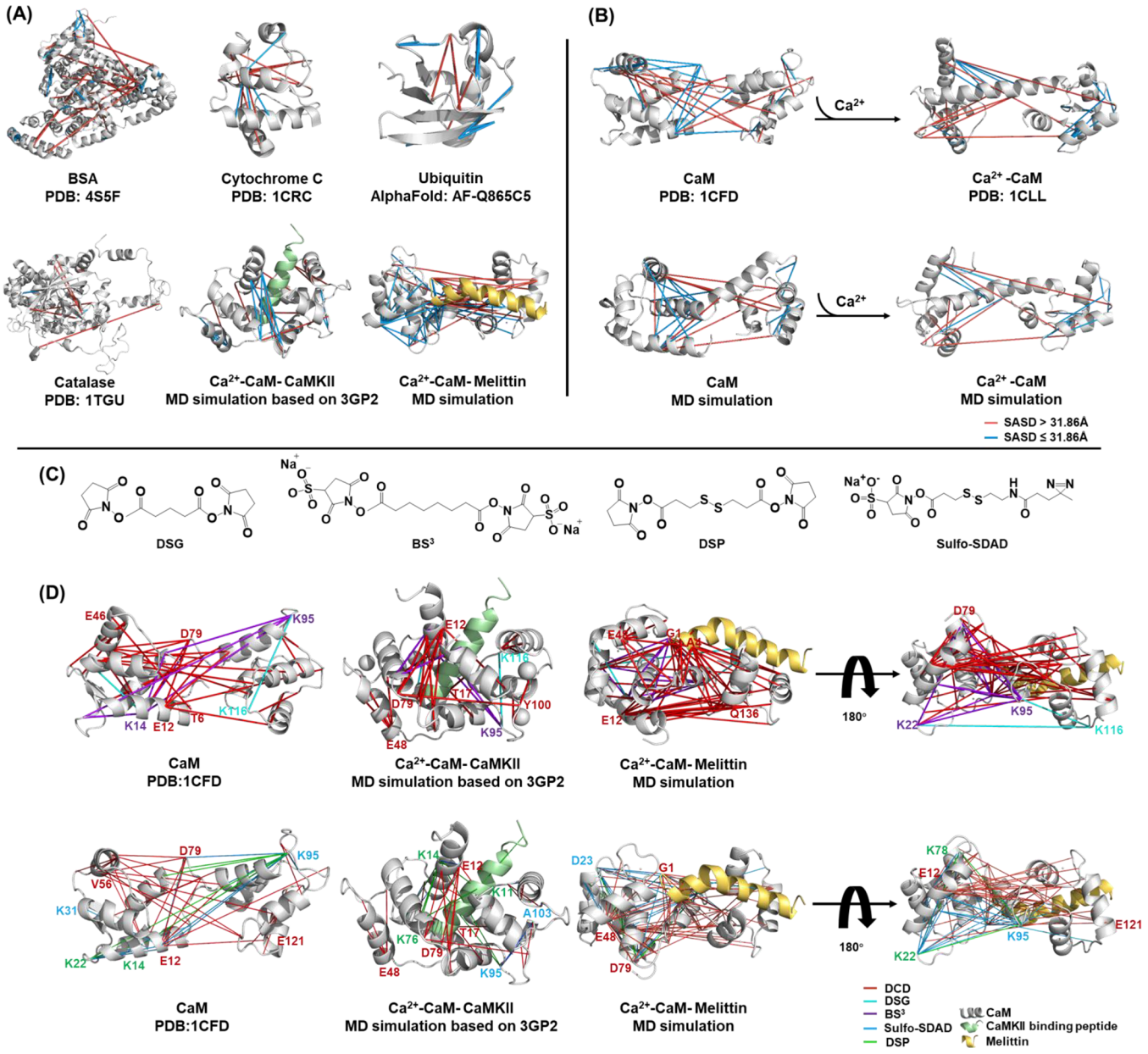

Figure 3. DCD cross-linking of (A) model proteins and protein complexes; blue lines indicate cross-links having SASD ≤31.86 Å, and orange red lines indicate cross-links having SASD > 31.86 Å. (B) CaM in Ca^{2+}-free and Ca^{2+}-binding states. Top panel: cross-links mapped on PDB structures; bottom panel: structures from MD simulation under the guidance of cross-links. Blue lines indicate cross-links having SASD ≤31.86 Å, and orange red lines indicate cross-links having SASD >31.86 Å. (C) Chemical structures of DSG, BS^3, DSP, and sulfo-SDAD. (D) CaM and its complexes with target peptides, cross-linked by DCD, BS^3, DSG, DSP, and sulfo-SDAD. Cross-linking constraint: BS^3 = 24.55 Å; DSG = 20.68 Å; DSP = 25.45 Å; and sulfo-SDAD = 29.28 Å.

supported the rationality of our developed cross-link identification strategy. Therefore, xiSEARCH with four-level FDR <5% was applied for DCD cross-link product identification and manual check would be required if necessary.

DCD Cross-linking of Protein and Protein Complex. We verified DCD cross-linking by using model proteins and protein complexes. Cross-links were identified by xiSEARCH and mapped to structures from PDB or AlphaFold. DCD cross-linking of BSA and CaM-complexes generated more cross-link products than that for cytochrome C, ubiquitin, and catalase (Figure 3A and Table S3). Of note, the molecular sizes of cytochrome C and ubiquitin are similar to that of CaM; therefore, the efficiency of DCD cross-linking was determined not only by the size of protein but also by other physiochemical properties such as the structural compactness, flexibility, and hydrophobicity, and the cross-linking constraint should also be considered. For Ca^{2+}−CaM−CaMKII binding peptide interaction, residues A13 and K17 of the CaMKII binding peptide formed intermolecular cross-links with CaM (Figure 3A and Table S4). This, along with numerous intra-CaM cross-links (Table S5), suggested a compact CaM conformation that wraps the CaMKII binding peptide, aligning with the structure determined by X-ray crystallography. In contrast, for the CaM−melittin complex, melittin formed intermolecular cross-links with CaM at multiple sites (Figure 3A and Table S4). Due to the lack of a crystal structure, Ca^{2+}−

https://doi.org/10.1021/acs.analchem.4c04939
Anal. Chem. 2025, 97, 5488−5497

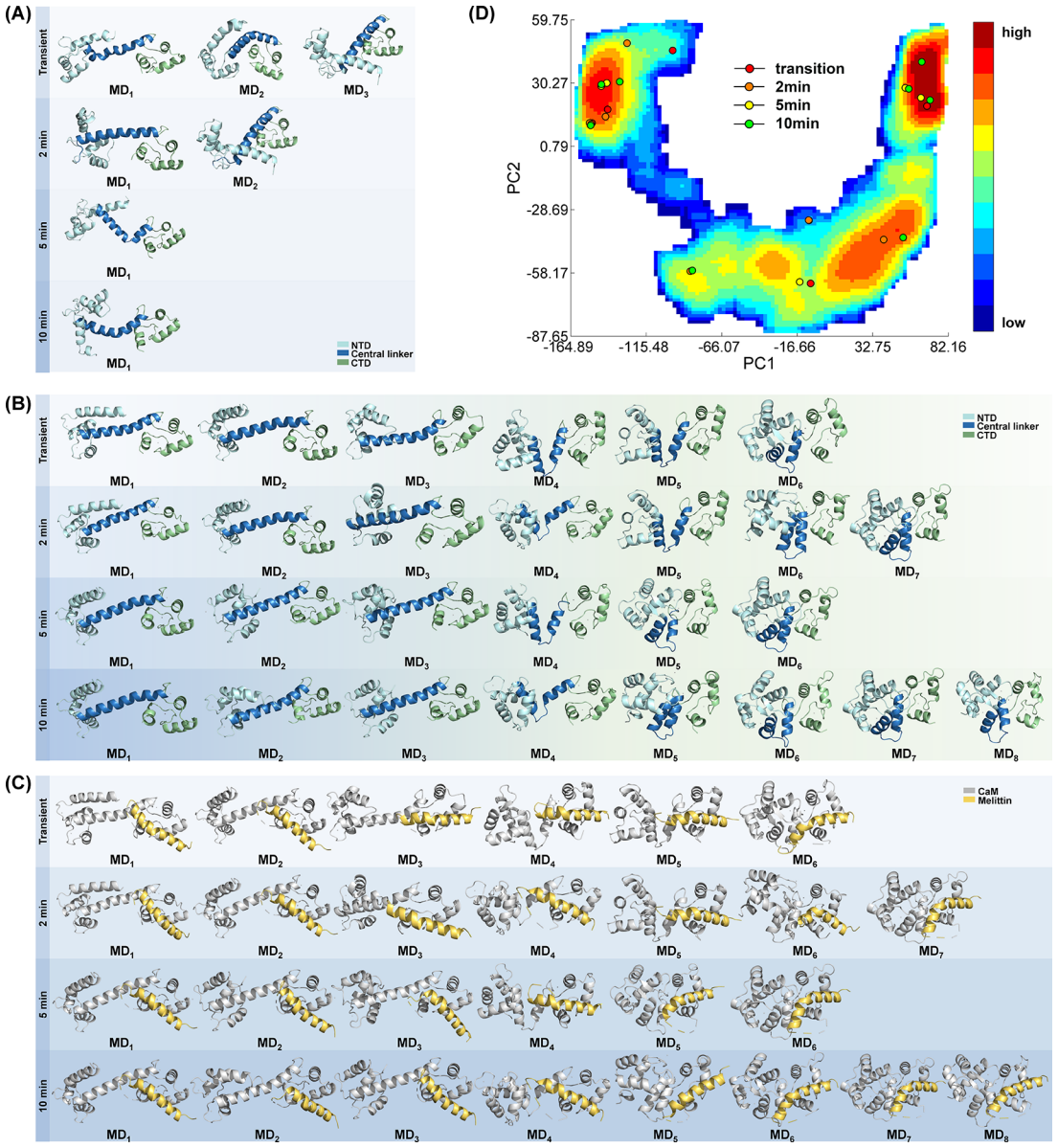

Figure 4. Conformational snapshots of CaM (A) induced by Ca^{2+} binding. (B) Induced by melittin interaction. (C) Conformational snapshots of the CaM−melittin complex. (D) Heatmap computed with principal component analysis (PCA) based on MD simulation. Note: intermediate conformers of CaM and the corresponding complex were obtained by MD simulation according to cross-link products.

CaM (PBD 1CLL) was used as a template and SASD measurement revealed that abundant overlength cross-links clustered between the two domains of CaM, proposing a different interaction pattern (Table S6). MD simulation revealed a distinct, more stretched conformation of CaM induced by melittin, allowing SASD of more cross-link products to fall within the DCD cross-linking constraint (Table S6). Melittin was found to fit into the C-terminal domain (CTD) cavity and its N-terminal oriented toward the central linker and the N-terminal domain (NTD) of CaM (Figure 3A).

Results also showed that a proportion of cross-links surpassed the DCD cross-linking constraint (32.7% for BSA and 47.6% for CaM in the complex with the CaMKII binding peptide, Tables S3 and S5) when mapped to crystal structures, highlighting alternative in-solution conformations and the dynamic nature of proteins. Taking CaM in the Ca^{2+}-free state as an example, NTD formed abundant cross-links with the central linker and the CTD, indicative of their spatial proximity, and a "closed-state" conformation agreed with the crystal structure (Figure 3B, top panel, and Table S7). As a result of Ca^{2+} binding, an "open-state" conformation was formed, as indicated by a decrease in between-domain cross-links. The increased number of cross-links within the CTD indicated its compression (Figure 3B, top panel, and Table S7). In the Ca^{2+}-free state, 59.3% of cross-links had SASDs within the cross-linking constraint of DCD, which was lower than the results obtained in the Ca^{2+}-binding state (71.4% of cross-links within the DCD cross-linking constraint), likely due to the stabilization effect of Ca^{2+} binding, which resulted in a less flexible structure compared to that observed in the Ca^{2+}-free state. MD simulation provided an alternative conformation for Ca^{2+}-free CaM, which increased the proportion of cross-links that fell within the DCD cross-linking constraint to as high as 74.1% (Figure 3B, bottom panel, Table S7), having a more spherical NTD and CTD, along with a more helical

https://doi.org/10.1021/acs.analchem.4c04939
Anal. Chem. 2025, 97, 5488−5497

central linker.[13,28] Differently, Ca^{2+}-binding CaM from MD simulation resulted in a similar number of overlength cross-links (9 out of 28, Figure 3B, bottom panel, and Table S7) with that mapped to the crystal structure (8 out of 28, based on PDB 1CLL, Table S7), confirming structural stability by Ca^{2+} binding.

Cross-linking of DCD vs Site-Specific Cross-linkers. Taking CaM and its complex with target peptides as examples, we assessed the performance of DCD cross-linking against four typical cross-linkers, namely, NHS ester homobifunctional cross-linkers BS^3, DSG, and DSP and one heterobifunctional cross-linker sulfo-SDAD (chemical structures in Figure 3C). In the case of CaM cross-linking, structural information obtained from NHS ester homobifunctional cross-linkers was limited as they cross-linked between lysine residues only. Sulfo-SDAD cross-linked more sites as expected by ligating lysine to any other adjacent amino acids. In comparison, DCD cross-linking provided overlapping structural information with that obtained from other cross-linkers. Moreover, the two diazirines of DCD fully released the reaction selectivity, thereby creating more sites that were not accessible to the other cross-linkers. Furthermore, the investigation of SASD measurements based on the PDB structure revealed that 59.3% of cross-links were within the cross-linking range of DCD, which was higher than that obtained from BS^3, DSG, DSP, and sulfo-SDAD cross-linking (Figure 3D and Tables S7 and S8).

DCD cross-linking also performed well with the CaM−CaMKII binding peptide complex, whereas the other four cross-linkers hardly produced intermolecular cross-links. It was probably due to unsuitable inter-residue distances or a lack of linkable sites within the cross-linking range. Similar for the CaM−melittin complex, no intermolecular cross-links were detected with DSG and DSP cross-linking. BS^3 and sulfo-SDAD cross-linking offered intermolecular cross-links but were less effective, which was limited by targetable lysine residues. As shown, DCD was more effective than the other cross-linkers, demonstrating its potential and capacity to provide complementary structural insights by enhancing cross-link coverage and improving the spatial resolution (Figure 3D and Tables S4 and S9).

Protein Dynamic Analysis by Transient Cross-linking Mass Spectrometry. CaM detects diverse Ca^{2+} signals and modulates the biological functions of numerous targets.[29] Its conformational dynamics are crucial for responding to Ca^{2+} signals and for interacting with other proteins to fulfill its biological roles.[30,31] Its structures in Ca^{2+}-free and Ca^{2+}-bound states have been well resolved; however, its conformational dynamics and coexistence of metastable states induced by Ca^{2+} binding remain unclear.

Taking advantage of transient cross-linking of DCD, a significant local conformational change in the CTD of CaM was observed by cross-linking at the very moment of Ca^{2+} addition. It was evidenced by an increase in the number of cross-links within this domain and its cross-linking with the central linker, as compared to the cross-linking in the Ca^{2+}-free state (Table S7), which was consistent with previously reported results.[32] Meanwhile, the NTD was less compact and positioning away from the central linker by observing the decrement of cross-links within the NTD and its linking with the central linker, respectively (Table S10). MD simulation revealed that one single model hardly accommodated all overlength cross-links due to the conformational heterogeneity captured by chemical cross-linking.[33] We explored more in the conformational ensemble and found three complementary conformers that allowed the greatest number of overlength cross-links to become DCD cross-linkable (24 out of 28 were covered) (Figure 4A and Table S10, at the transient time point). These comparative models highlight that CaM responds rapidly to Ca^{2+} binding and forms a highly flexible central linker and a dynamic CTD. At the 2 min time point, the cross-linking patterns observed within NTD and its interaction with the central linker were comparable to those in the Ca^{2+}-free state, implying a spatial fluctuation between the NTD and the central linker. A more compact CTD was characterized by detecting more cross-links within it (Tables S7 and S10 at the 2 min time point). Two intermediate conformers were obtained by MD simulation, including one stretched (MD_1 in Figure 4A, 2 min) and one closed (MD_2 in Figure 4A, 2 min), revealing a sphere-shaped CTD while the NTD moved around the central linker. CaM was approaching dynamic equilibrium at 5 min and after by yielding similar cross-link results. CaM was proposed to present the expected open conformation, as indicated by losing most between-domain cross-links. Also notable is that one conformational snapshot was structurally compatible with cross-links at 5 and 10 min (Figure 4A and Table S10, at 5 and 10 time points), confirming that CaM was nearly conformationally stable after 5 min of Ca^{2+} binding.

In the presence of target, using melittin as a representative example, CaM experienced a distinct conformational change and MD simulation provided six possible intermediate conformers to cover cross-links, three of which closely resemble those observed during Ca^{2+} binding (Figure 4B, MD_{1-3} at the transient time point), as evidenced by the presence of a helical central linker and more dumbbell NTD and CTD. In addition, CaM adopted three additional different conformations carrying an uncoiled central linker and folding to a spherical conformation (Figure 4B, MD_{4-6} at the transient time point). The proportion of these conformations increased from 50 to 62% along with the melittin binding (Figure 4B, MD_{4-7} at 2 min, MD_{4-6} at 5 min, and MD_{4-8} at 10 min), as evidenced by the increased number of between-domain cross-links (Table S11).

The detection of intermolecular cross-links revealed that, at the very moment of Ca^{2+} addition, multiple sites within CaM, predominantly in the NTD and CTD, formed cross-links with melittin, ranging from G1 to V5 (Table S12). MD simulation implies a potential interaction model where melittin approaches the CTD of CaM (Figure 4C). Their interaction was getting closer according to the continuously increased number of intermolecular cross-links and was eventually stabilized at 5 min after Ca^{2+} binding, as evidenced by the similar intermolecular cross-links detected at the 5 and 10 min time points (Table S12). These results also suggest that melittin approaches the CTD upon Ca^{2+} binding, the central linker uncoils, and CaM undergoes transition to the spherical state, which is conducive to wrapping around and stabilizing the target interaction. Additionally, the distribution of representative structures at each time point was consistent with the timeline of MD simulations (Figure 4D), confirming the reliability of our transient cross-linking. Notably, a few conformers appeared in the unexpected time region, which was probably due to the highly dynamic nature of proteins in solution, and more cross-linking information would be beneficial for modeling if available. Moreover, the integration of SASD of cross-linked residues and DCD cross-linking

https://doi.org/10.1021/acs.analchem.4c04939
Anal. Chem. 2025, 97, 5488−5497

constraints derives spatial proximity information and underscores the conformational heterogeneity, which aids in visualizing the coexistence of conformational intermediates.

CONCLUSIONS

This study highlights DCD as a novel cross-linker for protein dynamic analysis. The diversity of cross-linking sites facilitates high-resolution structural analysis, providing a detailed view of protein conformations. The transient cross-linking feature of DCD, enhanced by sample freezing, enables us to capture conformational snapshots and substantiates the coexistence of conformational intermediates. Consequently, the developed transient cross-linking MS method is promising for addressing how variations in protein conformation regulate its function, offering new insights into the complex interplay between structure and function, demonstrating the significant potential for monitoring conformational dynamics, and paving the way for new discoveries in structural biology.

Despite its effectiveness, ongoing work is essential to improve its performance and applicability, especially for complex systems. Progress in computational power, data analysis, and sample preparation will unlock the full potential for studying protein dynamics and interactions. For future studies with complex samples (e.g., living cell cross-linking), larger databases would expand the search space and analysis time, possibly increasing the false positives. Implementing an enrichment strategy (e.g., size exclusion chromatography or cation enrichment[15]), or designing an enrichment handle,[19] is a legitimate next step to simplify complex sample analysis. Cloud-based database searches could also optimize and expedite the search process. Additionally, improving cross-linking efficiency may lead to overcross-linking, which could increase nonspecific cross-links and generate false-positive results, thereby interfering with the genuine analysis of protein dynamics and interactions, masking or confusing the variety of protein conformational changes under different physiological conditions, and ultimately compromising the reliability of the data. Future work should also focus on establishing an evaluation standard by controlling the extent of cross-linking to ensure structural reliability and minimizing overcross-linking-induced structural perturbations, as well as improving the resolution of SASD and addressing the computational challenges of MD simulations.

ASSOCIATED CONTENT

Supporting Information

The Supporting Information is available free of charge at https://pubs.acs.org/doi/10.1021/acs.analchem.4c04939.

DCD cross-link identification by xiSEARCH; DCD cross-link products and cross-link sites; SASD measurements of cross-links; and cross-link products of BS^3, DSG, DSP, and sulfo-SDAD cross-linking (XLSX)

Experimental details, including additional reagents and chemicals, synthesis of DCD, lysozyme Coomassie blue staining, cross-linking methods for DSP, sulfo-SDAD, DSG, and BS^3, cell culture and cell lysate preparation, protein digestion and LC-MS analysis, data processing, protein structural modeling, and references; ^{1}H NMR and ^{13}C NMR spectra of DCD; MS and MS/MS spectra of DCD; MS spectra of DCD alone reacted under laser irradiation, DCD activation with the mixture of peptides SG and GK; possible reactions for the carbene generated by 4N elimination; MS spectra of the DCD-cross-linked peptide mixture; MS/MS spectra of corresponding interpeptide products; MS/MS spectra of representative cross-linked products; MS spectra of DCD-cross-linked lysozyme; and statistics of DCD modification sites based on cell lysate cross-linking (DOCX)

AUTHOR INFORMATION

Corresponding Authors

Huiyong Sun − *Department of Medicinal Chemistry, School of Pharmacy, China Pharmaceutical University, Nanjing, Jiangsu 210009, China*; orcid.org/0000-0002-7107-7481; Email: huiyongsun@cpu.edu.cn

Haiping Hao − *State Key Laboratory of Natural Medicines, Institute of Innovative Drug Discovery and Development, Jiangsu Provincial Key Laboratory of Targetome and Innovative Drugs, China Pharmaceutical University, Nanjing, Jiangsu 210009, China*; Email: haipinghao@cpu.edu.cn

Xiaowei Xu − *Institute of Innovative Drug Discovery and Development, China Pharmaceutical University, Nanjing, Jiangsu 210009, China*; orcid.org/0000-0003-1886-2728; Email: xw@cpu.edu.cn

Qiuling Zheng − *Department of Pharmaceutical Analysis, School of Pharmacy, China Pharmaceutical University, Nanjing, Jiangsu 210009, China*; orcid.org/0000-0003-1589-5591; Email: qiuling_zheng@cpu.edu.cn

Authors

Yuxin Xie − *Department of Pharmaceutical Analysis, School of Pharmacy, China Pharmaceutical University, Nanjing, Jiangsu 210009, China*

Jiawen Wang − *Department of Pharmaceutical Analysis, School of Pharmacy, China Pharmaceutical University, Nanjing, Jiangsu 210009, China*

Lei Yang − *Department of Pharmaceutical Analysis, School of Pharmacy, China Pharmaceutical University, Nanjing, Jiangsu 210009, China*

Junjun Tao − *Department of Pharmaceutical Analysis, School of Pharmacy, China Pharmaceutical University, Nanjing, Jiangsu 210009, China*

Yuanyuan Xu − *Department of Pharmaceutical Analysis, School of Pharmacy, China Pharmaceutical University, Nanjing, Jiangsu 210009, China*

Yang Hu − *State Key Laboratory of Natural Medicines, Institute of Innovative Drug Discovery and Development, Jiangsu Provincial Key Laboratory of Targetome and Innovative Drugs, China Pharmaceutical University, Nanjing, Jiangsu 210009, China*

Guiqing Zou − *State Key Laboratory of Natural Medicines, Institute of Innovative Drug Discovery and Development, Jiangsu Provincial Key Laboratory of Targetome and Innovative Drugs, China Pharmaceutical University, Nanjing, Jiangsu 210009, China*

Yu Su − *Department of Pharmaceutical Analysis, School of Pharmacy, China Pharmaceutical University, Nanjing, Jiangsu 210009, China*

Meijun Liu − *Department of Pharmaceutical Analysis, School of Pharmacy, China Pharmaceutical University, Nanjing, Jiangsu 210009, China*

Complete contact information is available at: https://pubs.acs.org/10.1021/acs.analchem.4c04939

https://doi.org/10.1021/acs.analchem.4c04939
Anal. Chem. 2025, 97, 5488−5497

Author Contributions

[1]Y.X., J.W., and L.Y. contributed equally to this study.

Notes

The authors declare no competing financial interest.

■ ACKNOWLEDGMENTS

This work was supported by the National Natural Science Foundation of China (grants 81930109 and 82321005); the Major State Basic Research Development Program of China (grant 2021YFA1301300); Overseas Expertise Introduction Project for Discipline Innovation (grant G20582017001); the Project of State Key Laboratory of Natural Medicines, China Pharmaceutical University (SKLNMZZ202402); Sanming Project of Medicine in Shenzhen (grant SZSM202301035) and Major Science and Technology Project of Jiangsu Province (BG2024045).

■ REFERENCES

(1) Wlodawer, A.; Minor, W.; Dauter, Z.; Jaskolski, M. *FEBS J.* **2013**, *280* (22), 5705−5736.
(2) Danev, R.; Yanagisawa, H.; Kikkawa, M. *Trends Biochem. Sci.* **2019**, *44* (10), 837−848.
(3) Kajihara, D.; Abe, R.; Iijima, I.; Komiyama, C.; Sisido, M.; Hohsaka, T. *Nat. Methods* **2006**, *3* (11), 923−929.
(4) Nesmelov, Y. E. *Methods Mol. Biol.* **2014**, *1084*, 63−79.
(5) Tamara, S.; den Boer, M. A.; Heck, A. J. R. *Chem. Rev.* **2022**, *122* (8), 7269−7326.
(6) Wu, S.; Zhang, S.; Liu, C. M.; Fernie, A. R.; Yan, S. *Mol. Cell Proteomics* **2025**, *24* (1), No. 100887.
(7) Trabjerg, E.; Nazari, Z. E.; Rand, K. D. *TrAC, Trends Anal. Chem.* **2018**, *106*, 125−138.
(8) Liu, X. R.; Zhang, M. M.; Gross, M. L. *Chem. Rev.* **2020**, *120* (10), 4355−4454.
(9) Pan, X.; Limpikirati, P.; Chen, H.; Liu, T.; Vachet, R. W. *J. Am. Soc. Mass Spectrom.* **2020**, *31* (3), 658−665.
(10) Mendoza, V. L.; Vachet, R. W. *Anal. Chem.* **2008**, *80* (8), 2895−2904.
(11) Iacobucci, C.; Götze, M.; Sinz, A. *Curr. Opin. Biotechnol.* **2020**, *63*, 48−53.
(12) Wang, J.-H.; Tang, Y.-L.; Gong, Z.; Jain, R.; Xiao, F.; Zhou, Y.; Tan, D.; Li, Q.; Huang, N.; Liu, S.-Q.; Ye, K.; Tang, C.; Dong, M.-Q.; Lei, X. *Nat. Commun.* **2022**, *13* (1), 1468.
(13) Ding, Y. H.; Gong, Z.; Dong, X.; Liu, K.; Liu, Z.; Liu, C.; He, S. M.; Dong, M. Q.; Tang, C. *J. Biol. Chem.* **2017**, *292* (4), 1187−1196.
(14) Zheng, Q.; Zhang, H.; Tong, L.; Wu, S.; Chen, H. *Anal. Chem.* **2014**, *86* (18), 8983−8991.
(15) Yu, C.; Huang, L. *Anal. Chem.* **2018**, *90* (1), 144−165.
(16) Gutierrez, C. B.; Block, S. A.; Yu, C.; Soohoo, S. M.; Huszagh, A. S.; Rychnovsky, S. D.; Huang, L. *Anal. Chem.* **2018**, *90* (12), 7600−7607.
(17) Müller, F.; Graziadei, A.; Rappsilber, J. *Anal. Chem.* **2019**, *91* (14), 9041−9048.
(18) Belsom, A.; Mudd, G.; Giese, S.; Auer, M.; Rappsilber, J. *Anal. Chem.* **2017**, *89* (10), 5319−5324.
(19) Zhang, B.; Gao, H.; Gong, Z.; Zhao, L.; Zhong, B.; Sui, Z.; Liang, Z.; Zhang, Y.; Zhao, Q.; Zhang, L. *Anal. Chem.* **2023**, *95* (25), 9445−9452.
(20) Gomes, A. F.; Gozzo, F. C. *J. Mass Spectrom.* **2010**, *45* (8), 892−899.
(21) Yuan, S.; Xia, L.; Wang, C.; Wu, F.; Zhang, B.; Pan, C.; Fan, Z.; Lei, X.; Stevens, R. C.; Sali, A.; Sun, L.; Shui, W. *ACS Cent. Sci.* **2023**, *9* (5), 992−1007.
(22) Wang, J.; Burdzinski, G.; Kubicki, J.; Platz, M. S.; Moss, R. A.; Fu, X.; Piotrowiak, P.; Myahkostupov, M. *J. Am. Chem. Soc.* **2006**, *128* (51), 16446−16447.
(23) Iacobucci, C.; Goetze, M.; Piotrowski, C.; Arlt, C.; Rehkamp, A.; Ihling, C.; Hage, C.; Sinz, A. *Anal. Chem.* **2018**, *90* (4), 2805−2809.
(24) Matzinger, M.; Vasiu, A.; Madalinski, M.; Müller, F.; Stanek, F.; Mechtler, K. *Nat. Commun.* **2022**, *13* (1), 3975.
(25) Chen, Z.-L.; Meng, J.-M.; Cao, Y.; Yin, J.-L.; Fang, R.-Q.; Fan, S.-B.; Liu, C.; Zeng, W.-F.; Ding, Y.-H.; Tan, D.; Wu, L.; Zhou, W.-J.; Chi, H.; Sun, R.-X.; Dong, M.-Q.; He, S.-M. *Nat. Commun.* **2019**, *10* (1), 3404.
(26) Mendes, M. L.; Fischer, L.; Chen, Z. A.; Barbon, M.; O'Reilly, F. J.; Giese, S. H.; Bohlke-Schneider, M.; Belsom, A.; Dau, T.; Combe, C. W.; Graham, M.; Eisele, M. R.; Baumeister, W.; Speck, C.; Rappsilber, J. *Mol. Syst. Biol.* **2019**, *15* (9), No. e8994.
(27) Belsom, A.; Schneider, M.; Fischer, L.; Brock, O.; Rappsilber, J. *Mol. Cell. Proteomics* **2016**, *15* (3), 1105−1116.
(28) Zhang, B.; Gong, Z.; Zhao, L.; An, Y.; Gao, H.; Chen, J.; Liang, Z.; Liu, M.; Zhang, Y.; Zhao, Q.; Zhang, L. *Angew. Chem., Int. Ed. Engl.* **2023**, *62* (35), No. e202301345.
(29) Zhang, M.; Abrams, C.; Wang, L.; Gizzi, A.; He, L.; Lin, R.; Chen, Y.; Loll, P. J.; Pascal, J. M.; Zhang, J. F. *Structure* **2012**, *20* (5), 911−23.
(30) Tran, O.; Kerruth, S.; Coates, C.; Kaur, H.; Peracchia, C.; Carter, T.; Török, K. *Int. J. Mol. Sci.* **2023**, *24* (4), 4153.
(31) Ulke-Lemée, A.; Ishida, H.; Chappellaz, M.; Vogel, H. J.; MacDonald, J. A. *Biochim. Biophys. Acta* **2014**, *1844* (9), 1580−90.
(32) Halling, D. B.; Aracena-Parks, P.; Hamilton, S. L. *Sci. STKE* **2005**, *2005* (315), re15.
(33) Ferber, M.; Kosinski, J.; Ori, A.; Rashid, U. J.; Moreno-Morcillo, M.; Simon, B.; Bouvier, G.; Batista, P. R.; Müller, C. W.; Beck, M.; Nilges, M. *Nat. Methods* **2016**, *13* (6), 515−520.

https://doi.org/10.1021/acs.analchem.4c04939
Anal. Chem. 2025, 97, 5488−5497